Density functional theory with hybrid functionals applied to defects in GaAs surfaces: Effect of doping

H. Williams and W. A. Hofer*
Surface Science Research Centre, The University of Liverpool, Liverpool L69 3BX, United Kingdom

E. Ćavar, A. Mikkelsen, and E. Lundgren
Department of Physics, Synchrotron Radiation Research, Lund University, P.O. Box 118, S-221 00 Lund, Sweden

(Received 25 June 2008; revised manuscript received 11 September 2008; published 10 November 2008)

We have analyzed the influence of a Ga vacancy on electronic properties of GaAs(110) by scanning tunneling microscopy (STM), *ab initio* electronic structure simulations based on density functional theory with Perdew-Becke-Ernzerhof and Heyd-Scuseria-Ernzerhof functionals and STM simulations. We find that the HSE03 functional improves the description of the band gap of the semiconductor surface in line with recent bulk simulations. The inclusion of doping in the crystal significantly affects the position of the band gap in the electronic structure and the signature of the defect. The simulated STM images show good correlation with the main features of the experimental images only for hybrid-functional simulations and only if the effects of doping and band bending are included in the description.

DOI: 10.1103/PhysRevB.78.205309 PACS number(s): 73.20.At, 68.37.Ef

I. INTRODUCTION

A number of present and future applications of semiconductor technology rely on the unique properties of the III-V semiconductors such as gallium arsenide. Due to the wide range of the III-V materials, and the possibility to combine them into more complex compounds, they are among the favorites for nanoscale engineering. The addition of atomic scale defects allows the engineering of specific electronic properties by inducing states within the band gap.[1–8] However, for these states to be utilized, the detailed electronic structure of the system needs to be known.

There are three key problems facing a theoretical model of such a system: (i) the fundamental problem in density functional theory (DFT) of the underestimation of band gaps in semiconductors. In plane-wave codes, this problem could only recently be overcome by the introduction of hybrid functionals with a finite decay length. (ii) The fundamental problem of semiconductor doping. While this usually only leads to small errors in the position of the Fermi level, an error which can furthermore be corrected by placing the Fermi level at a specific position within the band gap, it can lead to quite substantial errors as soon as specific defects are involved. In this case the subtle balance between doping levels and defects, in conjunction with the long decay lengths within semiconductors, will yield most simulations somewhat less than trustworthy. (iii) Finally, the electronic structure of the semiconductor will change locally due to the field of a probe tip. These band bending effects can be included in a continuum model of the semiconductor,[4,7] but they are still somewhat beyond the reach of atomistic and first-principles simulation methods. That they must play a role is quite obvious if a defect state is not detected at low tunneling bias—where it will be positioned in energy space according to band-structure simulations—but either at or below the onset of the valence band or above the onset of the conduction band.

In this work we report the results of scanning tunneling microscopy (STM) studies of a Ga vacancy on a GaAs(110) surface. *Ab initio* simulations are carried out and compared to STM measurements and dI/dV spectra. For the DFT simulations[9,10] we used two different exchange-correlation functionals: a Perdew-Becke-Ernzerhof (PBE) functional[11] and the Heyd-Scuseria-Ernzerhof (HSE03) (Refs. 12 and 13) functional. This (hybrid) functional is found to significantly improve the description of the band gap of the semiconductor surface, in line with recent bulk simulations.[14,15] However, it does not solve the problem of the onset of defect states at the vacancy, evident in STM scans. To this end we resort to a semiempirical scheme describing band bending.

II. METHOD

A. Experiment

Experiments were performed in an Omicron UHV STM operating at room temperature with a base pressure of 2×10^{-11} mbar. Samples, silicon doped GaAs(100) wafers with carrier concentration of 3.4×10^{18} cm^{-3} and resistivity of 1.2×10^{-3} Ohm/cm were cleaved in UHV exposing clean (110) surface. Atomically resolved STM topographies shown here were obtained in the constant current imaging mode using etched tungsten tips, cleaned by Ar^+ sputtering. The voltages indicated are the voltage on the sample, thus with a positive sample voltage electrons tunnel to the sample (into empty states) while at negative voltages electrons will tunnel from the sample (from filled states). dI/dV spectra were obtained as single spectra with no spectra averaging and with an open feedback loop while tip was held at constant distance from the GaAs surface above a selected point.

Figure 1 shows STM images obtained at different bias voltages from −3 to +3 V. At a negative bias, the As atoms appear as protrusions in the STM image due to tunneling from As derived states to the tip.[16–18] Furthermore, the Ga vacancy appears as a two-lobed bright protrusion along the As row under these conditions, as already observed in previous studies.[19] Under positive bias electrons tunnel from the

 ©2008 The American Physical Society

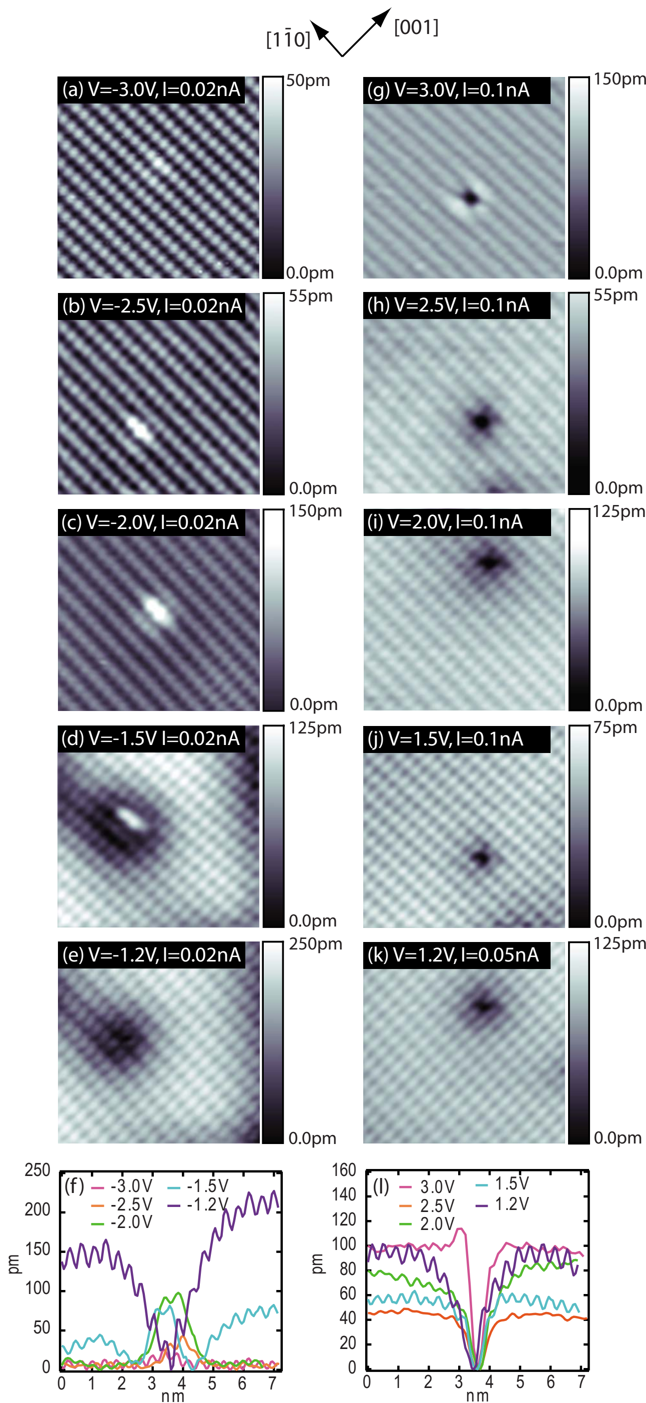

FIG. 1. (Color online) (Top frames) Atomically resolved STM images of the GaAs(110) surface showing Ga vacancy at [(a)–(e)] negative sample voltages and at [(g)–(k)] positive sample voltages. STM images size is 7.5×7.5 nm^2. (f) and (l) show line profiles along the [1–10] direction across Ga vacancy at negative and positive sample voltages, respectively.

tip into empty Ga-related states, revealing the Ga atoms as protrusions in the STM image. Under these conditions, the vacancy appears as a depression along the Ga rows. By plotting line scans from the images across the defects, the apparent height variations can be followed as shown in the bottom frames of Fig. 1 (a–f: negative bias; g–l: positive bias). The plots show that the intensity due to the defect peaks around −2 V, and decreases at lower negative voltages. At positive biases the defect is observed as a depression with a similar apparent depth over a wide voltage range, it is not until the bias voltage reaches around +3 V that the depth of the depression starts to diminish.

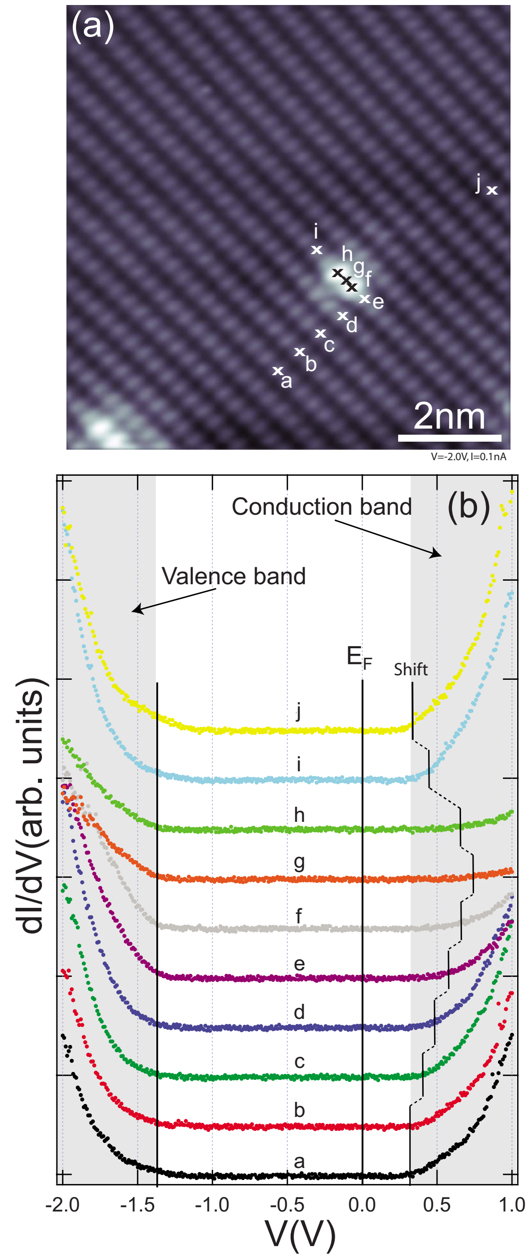

FIG. 2. (Color online) (a) STM image of the GaAs(110) surface with Ga vacancies recorded using a sample voltage of −2 V. Points *a–j* indicate positions at which tunneling spectra were recorded. (b) Tunneling spectra from points *a–j* as indicated in (a). The shift of the onset of the conduction band as the position of the tip is moved is indicated.

By performing tunneling spectroscopy at the defect and comparing to spectroscopy obtained from the regular GaAs(110) surface, more information on the contrast mechanism as described above can be obtained. Figure 2(a) shows a STM image of the GaAs(110) surface with Ga vacancies

obtained for the tunneling voltage of −2 V and current of 0.1 nA. In the image, several points, from *a* to *j*, are indicated at which tunneling spectroscopy was performed. The corresponding spectra are shown in Fig. 2(b). From the spectra, it can be concluded that the dI/dV contributions are higher in the negative bias regime at which the defect appears as a strong protrusion in Fig. 2(a). Similarly, in the positive bias regime, the dI/dV contribution from the regular GaAs(110) surface is higher than that from the defect, explaining the observed depression. The variation in the appearance of the defect shown in Fig. 1 is therefore in complete agreement with the spectra shown in Fig. 2(b).

Turning to the onset of the conduction band, as expected in an *n*-type semiconductor such as Si doped GaAs, the onset of the conduction band is shifted toward higher energy with respect to the Fermi level [corresponding to 0 V in the dI/dV spectra in Fig. 2(b)].[19] This behavior can be seen in all spectra; at the clean GaAs(110) surface far away from the defect as well as at the defect.

However, as the location of the spectroscopy point approaches the defect [going from *a* to *e* in Fig. 2(b)], the conduction band shifts further away from the Fermi level. The maximum shift with respect to the Fermi level is around 0.45 eV. The location of the maximum shift is exactly at the Ga vacancy [point *g* in Fig. 2(b)], although the shifts observed at the two As atoms closest to the Ga vacancy (points *f* and *h*) have a similar value. When the tip is again moved away from the defect site [points *i* and *j* in Fig. 2(b)], the onset of the conduction band shifts back toward that of the clean *n*-type GaAs surface. This behavior is also expected since the Ga vacancy represents a dopant with an *n* type of character. As the tip is approaching the Ga vacancy, the local effect of the *n* doping is increasing, having its maximum at the exact location of the vacancy [point *g* in Fig. 2(b)], resulting in the largest shift of the conduction band onset. In the valence band, no such significant shift can be seen; only a slightly shifted onset of the valence band toward the Fermi level can be detected.

In summary, while the tunnel spectra at the defect reveal the local characteristic of an *n*-doped semiconductor, the occurrence of the defect substantially shifts the conduction band to higher energy levels and thus increases the band gap locally. From a physical perspective the change in the local electronic structure must be due to the combination of two different physical effects: (i) the local charging of the surface due to the doping of the crystal;[4] (ii) the interaction with the defect altering the electrostatic potential and thus the band structure at the location of the defect. In addition, local band bending will also come into play as the STM tip field changes the electrostatic potential near the surface of the GaAs crystal. A detailed understanding of the interplay between these effects cannot be obtained by a simple ground-state DFT simulation since the calculation in this case does not give a correct representation of the electronic structure itself. In this case it is quite impossible to gauge the importance of the effects in a quantitative manner. However, an appropriate model simulation of the electronic ground state can serve as a point of reference, while the different effects are successively included by suitable adjustments of the model.

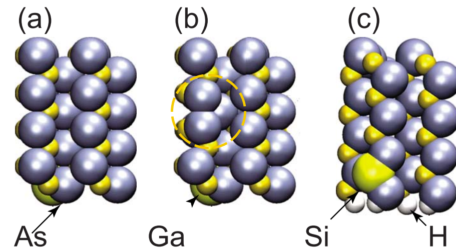

FIG. 3. (Color online) Unit cells used for the simulations. (a) shows the clean GaAs(110) surface. (b) shows the unit cell with the Ga vacancy defect. The atoms have been relaxed to their optimum positions for this setup. (c) shows the side view of the unit cell with the Si dopant replacing Ga in the seventh layer, and the bottom layer passivated by hydrogen.

B. Simulations

The unit cell in the simulations consisted of eight layers of a (2×4) GaAs(110) surface cell is shown in Fig. 3. The bottom layer was saturated by hydrogen. Figure 3(a) shows the clean GaAs(110) surface, with the atoms in their final positions. Figure 3(b) shows the unit cell containing the gallium vacancy at the surface. Also in this case the cell has been fully relaxed and the positions of the remaining surface atoms have shifted. We performed ionic relaxations only at the PBE level. However, checking a single simulation using HSE03 functionals, we found that the ionic positions remained close to their PBE values, with deviations of less than 2 pm. Initial electronic simulations were also carried out using PBE (Ref. 11) functionals within the projector augmented wave (PAW) (Ref. 9) method. The PBE functional is well known to underestimate the band gap of semiconductors,[14,15] the simulated electronic structure is therefore not well represented. Consequently, the PBE functionals cannot be expected to give satisfactory agreement between experimental and simulated STM scans.

To improve the electronic simulation of the semiconductor, a hybrid functional (HSE03) was used. This functional admixes DFT with a certain amount of Hartree-Fock (HF) exchange. A screened Coulomb potential is used for the HF exchange energy, reducing the long-range part of the HF energy to make it computationally tractable. The hybrid functional significantly improves the description of the electronic structure, including the band gap. The calculation time for a simulation using the hybrid functional is notably longer than that for an equivalent PBE calculation. The time for the calculations is no longer out of reach of modern computers, but does considerably limit the size of a system that can be calculated.

In a final step we chemically doped the semiconductor system. It was found that charging the system, i.e., increasing the number of electrons, does not lead to significant changes in the electronic structure at the defect site, presumably due to charge delocalization and the effect of the compensating positive background. However, chemical doping, e.g., replacing Ga (three valence electrons) by Si (four valence electrons, *n* doped), leads to changes in the electronic structure which are in line with experimental data. Figure 3(c) shows the side view of the unit cell with a silicon atom replacing a

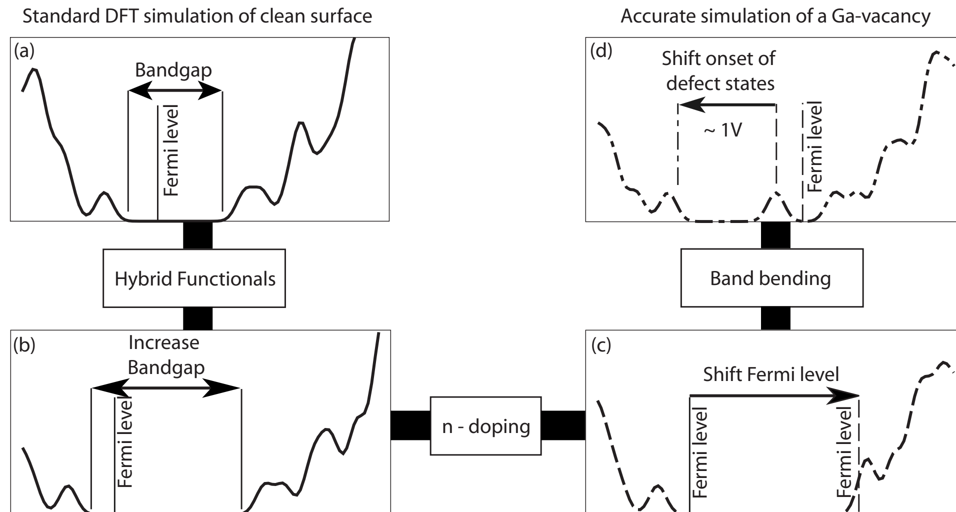

FIG. 4. Scheme of the simulation procedure. Starting from a clean GaAs(110) surface the (a) band gap in standard simulations is corrected by the use of a (b) HSE03 hybrid functional. (c) The position of the Fermi level in a doped semiconductor is then simulated by chemical doping of the system. (d) Finally, the bias-dependent weight of the defect states for a Ga vacancy shifts the onset of the visibility of these states to a position near the valence band or conduction band of the clean GaAs crystal. All steps are necessary to obtain quantitative agreement with experimental findings.

gallium atom, inducing *n* doping in the crystal. The Si atom was placed at the bottom of the unit cell so that it acts only as a dopant, but does not appear as a defect on the surface. Due to the small size of the unit cell, exchanging only one atom for Si induces a very high doping level of doping. Due to this feature, we may only expect qualitative agreement with experimental results. Also the position of the Si atom itself may lead to an asymmetric appearance of the defect, not fully in agreement with experiments. To achieve full quantitative agreement the doping level needs to be substantially lower. However, in view of hybrid functionals to compute the electronic structure, such a low doping level will remain firmly out of reach of *ab initio* simulations for some years to come.

The electronic states of each set of simulations were used to simulate STM scans using our standard simulation program, BSKAN.[20,21] Simulated images and apparent heights of surface features are then compared with the experimental results. Band bending is present at semiconductor surfaces due to the accumulation layer.[2,4,7] Given that the defect states at the Ga vacancy are in the band gap of the semiconductor (see further down), a bias voltage matching the energy level of the defect state should actually provide a current since the defect states will have a high density in the vacuum region above the surface. However, experimentally we observe these states at voltage levels which are at or below the value for the onset of the conduction band. Physically, this feature is only possible if the transition probability for electrons from the valence band into the defect states is close to zero at low bias values. Considering that at this bias the valence band will retain its energy position at the GaAs surface, the energy difference between the defect state and the valence-band edge will effectively reduce transition probability to a value close to zero. As the bias voltage increases, the STM tip field will penetrate the semiconductor and change the electrostatic potential at the GaAs surface. In this case, the energy eigenvalues of the defect states will decrease until they are below the valence-band edge of the bulk crystal. As a result, the transition probability will increase and eventually saturate at a specific negative bias. The same process will occur for positive bias and the conduction band. Theoretically, it is possible to calculate the effect of the tip field on the semiconductor electronic structure.[3,5–7] It was found that the current from the valence to the conduction band is comparable to the vacuum current for band gaps larger than about 1 V.[3] However, for smaller band gaps the interband transmission can substantially exceed the vacuum transmission, and in this case the dominant resistance in the STM is within the vacuum barrier. To account for the effect we have implemented a semiempirical treatment by varying the transition probability from the valence band into defect states between zero at low bias values and one at the saturation bias. Numerically, the variation was accounted for by a hyperbolic tangents, the parameters of the variation were adjusted so that the final simulated topographies match the experimental scans. The scheme of the simulation procedure as a successive implementation of hybrid functionals, doping, and band bending is shown in Fig. 4.

III. RESULTS AND DISCUSSION

The most important result in the experimental STM measurements is that at low negative bias voltage the Ga vacancy shows up as a depression. This depression changes into a protrusion at a defined threshold value of −1.2 V, reaches a peak apparent height difference at −2.0 V, and becomes almost invisible at −3.0 V (see Fig. 1). This feature is thus quite complicated, its level of complexity equal to the experimental results on Ge(111), which have recently been published.[5] However, from a physical point of view, the behavior is easy to understand if one considers, as above, that tunneling out of a defect state also depends on the transport

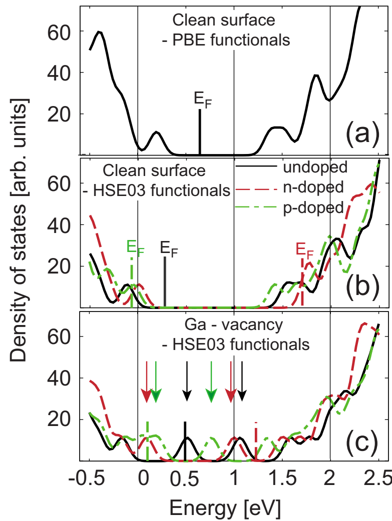

FIG. 5. (Color online) Density of states of the clean surface, using (a) PBE functionals and (b) HSE03 functionals. In frame (b) we also show the effect of substitutional doping: for *n*-doped material the Fermi level (vertical line) is shifted to the onset of the conduction band, for *p* doping to the onset of the valence band. Frame (c) shows the density of states for the defect. Depending on the doping the defect states are either fully occupied (*n* doping), of fully unoccupied (*p* doping). Arrows in frame (c) denote the position of defect states.

properties from the bulk valence band into the defect state and band bending due to the applied STM tip field. In this case the onset of the defect state signature will be retarded, i.e., shifted to lower energy values. Due to the localization of the defect states at the Ga vacancy these states will have a high density in the vacuum range and "light up" as soon as transport from the valence band becomes non-negligible. As more and more states of the surface contribute to the image, if the bias voltage is shifted to more negative values, the defect states will gradually vanish in the background of states from the valence band. In this scenario, the important information needed from a comparison with simulations is whether the appearance of defect states may also depend on doping of the crystal.

In Fig. 5 we show the density of states of the calculated systems. Comparing the results for different functionals, we note that the band gap for the PBE functional is about 1 eV, for the HSE03 functional about 1.4 eV, in line with experimental data. For the substitutional doping level possible within this first-principles simulations and including hybrid functionals, we find a very large shift of the Fermi level: for *p*-doped semiconductors the Fermi level is shifted to the onset of the valence band, for *n*-doped semiconductors to the onset of the conduction band. The defect states are, as one would expect, energetically positioned in the band gap; two nearly symmetric states for undoped GaAs and two states shifted toward the valence band (conduction band) for *n*-doped (*p*-doped) GaAs. As already analyzed in some detail above, these states (i) are within the band gap and (ii) should not leave a signature in the band gap in tunneling spectroscopies.

The images shown in Fig. 6 are the resulting STM simulations. Here, we have superimposed the simulated images of a clean GaAs(110) surface with one simulation containing the defect. Since the defect changes the property not only locally but depending on the size of the unit cell, throughout the system, we have also employed some smearing routing for the transitions from the defect unit cell to the clean surface cells. The simulation method successively takes the effects of doping and tip induced band bending into account. We find that the signature of the vacancy in a *p*-doped crystal would be at odds with experimental results and understandably so since the GaAs crystal in the experiments was *n* doped. However, that doping is crucial to obtain agreement is shown by the topography simulations of frames (a1) to (a3). In this case the crystal was not doped and the ensuing signature of the slight protrusion of less than 10 pm. at −2 V [frame (a1)], a slight depression at an adjacent site at −1 V [frame (a2)], and a depression at +1 V [frame (a3)]. Only the last simulation agrees with experiments. Substitutional doping not only changes the occupation of the defect states,[8] it also affects the electronic structure throughout the unit cell. This is seen in frames (b1) to (b3), which show the topographic images of the defect at −2 to +1 V. We find that the additional charge from the dopant will increase the signature of the defect in the negative bias regime as expected. While this trend is in line with experiments, the simulations at this stage do not account for transmission from defect states into the valence band and vice versa. The transmission coefficient in a multiple-scattering simulation[22] is only different from unity for transitions across the vacuum barrier. Unsurprisingly then, the defect is also simulated as a protrusion at −1 V, in contradiction with experiments. However, the most striking deviation from experiments is that this defect is simulated as a protrusion in the positive bias regime [frame (b3)]. Subsequently we have identified the defect states and weighted them with a bias-dependent weight. This procedure accounts for the tip induced bending of the valence band of GaAs(110). The two key variables in this semiempirical treatment of band bending are the onset voltage and the saturation voltage. The parameters chosen to account for the experiments were −1 and −2 V for the negative bias regime and +0.5 and +1.5 V for the positive bias regime. In physical terms this means that the model assumes that transmission from the valence band will become comparable with the tunneling transmission around −1 V and that it will reach a level close to unity at −2 V. The results of these simulations are shown in Fig. 6(c). These images agree well with experimental results. At −2.0 V, Fig. 6(c1), the defect is seen as a protrusion of about 100 pm. At −1.0 V, Fig. 6(c2), this protrusion has vanished and the defect is now evident as a depression on the clean surface. The same feature is found for measurements in to the positive bias regime at +2.0 V, Fig. 6(c3).

IV. CONCLUSIONS

We have investigated the Ga vacancy on the GaAs(110) surface using *ab initio* simulations and PBE and HSE03 functionals. We find that the HSE03 functionals significantly

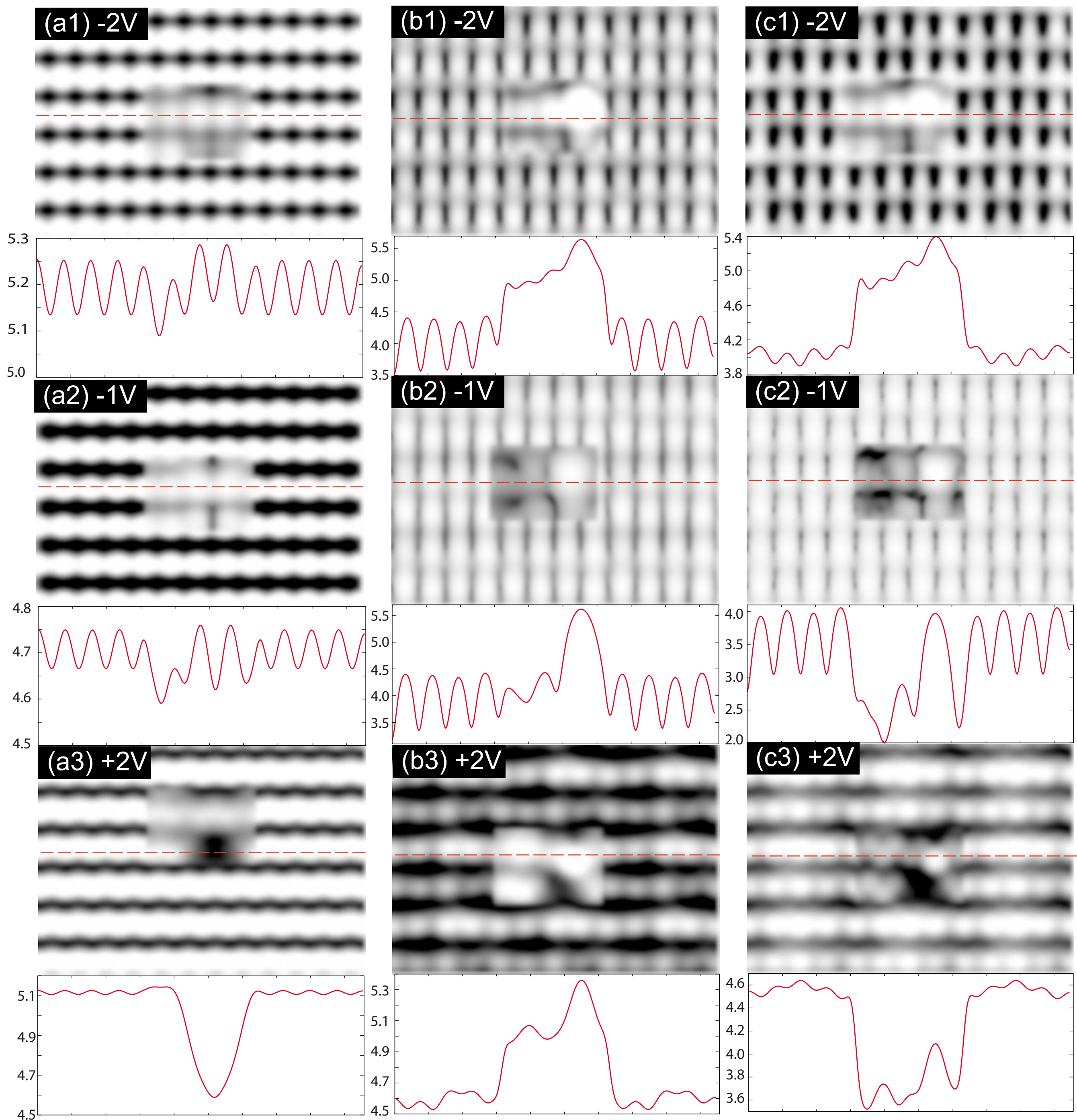

FIG. 6. (Color online) (a) Simulation results calculated with the HSE03 functional, (b) HSE03 functional including n doping in the crystal, and (c) HSE03 functional with n doping and the influence of band bending. Scans (1), (2), and (3) are carried out at −2, −1, and +2 V bias voltage, respectively.

improve the description of the band gap of the semiconductor surface, in line with recent bulk simulations. We also find that the appearance and the signature of defect states such as Ga vacancies on GaAs(110) are significantly changed by the doping level of the crystal. Furthermore, STM simulations show that band bending effects can actually be determined from the appearance of single defects in STM scans. In this respect we have found that two parameters, the onset of transmission from the valence or conduction band into defect states and the saturation bias are the key quantities for determining the results.

ACKNOWLEDGMENTS

This work was financially supported by EPSRC (H.W.), the Royal Society (W.A.H.), the Swedish Research Council (E.C.), the Crafoord foundation (A.M.), and the Knut and Alice Wallenberg foundation (E.L.).

*whofer@liverpool.ac.uk

[1] R. M. Feenstra, Phys. Rev. Lett. **63**, 1412 (1989).
[2] R. M. Feenstra and J. A. Stroscio, J. Vac. Sci. Technol. B **5**, 923 (1987).
[3] N. D. Jäger, E. R. Weber, K. Urban, and Ph. Ebert, Phys. Rev. B **67**, 165327 (2003).
[4] R. M. Feenstra, J. Vac. Sci. Technol. B **21**, 2080 (2003).
[5] R. M. Feenstra, S. Gaan, G. Meyer, and K. H. Rieder, Phys. Rev. B **71**, 125316 (2005).
[6] R. M. Feenstra, J. Y. Lee, M. H. Kang, G. Meyer, and K. H. Rieder, Phys. Rev. B **73**, 035310 (2006).
[7] R. M. Feenstra, Y. Dong, M. P. Semtsiv, and W. T. Masselink, Nanotechnology **18**, 044015 (2007).
[8] M. W. Radny, P. V. Smith, T. C. G. Reusch, O. Warschkow, N. A. Marks, H. F. Wilson, S. R. Schofield, N. J. Curson, D. R. McKenzie, and M. Y. Simmons, Phys. Rev. B **76**, 155302 (2007).
[9] P. E. Blöchl, Phys. Rev. B **50**, 17953 (1994).
[10] G. Kresse and J. Hafner, Phys. Rev. B **47**, 558 (1993); G. Kresse and D. Joubert, *ibid.* **59**, 1758 (1999).
[11] J. P. Perdew, M. Ernerzhof, and K. Burke, J. Chem. Phys. **105**, 9982 (1996).
[12] J. Heyd, G. E. Scuseria, and M. Ernzerhof, J. Chem. Phys. **124**, 219906 (2006).
[13] J. Paier, M. Marsman, K. Hummer, G. Kresse, I. C. Gerber, and J. G. Angyan, J. Chem. Phys. **125**, 249901 (2006).
[14] J. Heyd and G. E. Scuseria, J. Chem. Phys. **121**, 1187 (2004).
[15] J. Heyd, J. E. Peralta, G. E. Scuseria, and R. Martin, J. Chem. Phys. **123**, 174101 (2005).
[16] R. M. Feenstra, J. A. Stroscio, J. Tersoff, and A. P. Fein, Phys. Rev. Lett. **58**, 1192 (1987).
[17] G. J. de Raad, D. M. Bruls, P. M. Koenraad, and J. H. Wolter, Phys. Rev. B **66**, 195306 (2002).
[18] W. A. Hofer, K. Palotás, G. Teobaldi, J. Sadowski, A. Mikkelsen, and E. Lundgren, Nanotechnology **18**, 044006 (2007).
[19] Ph. Ebert, Surf. Sci. Rep. **33**, 121 (1999); Appl. Phys. A: Mater. Sci. Process. **75**, 101 (2002).
[20] W. Hofer and J. Redinger, Surf. Sci. **447**, 51 (2000).
[21] W. A. Hofer, Prog. Surf. Sci. **71**, 147 (2003).
[22] K. Palotás and W. A. Hofer, J. Phys.: Condens. Matter **17**, 2705 (2005).